Electronic Doping in Perovskite Solar Cells

Zuzanna Molenda, Sylvain Chambon, Dario M Bassani, Lionel Hirsch

ADVANCED ELECTRONIC MATERIALS Open Access
www.advelectronicmat.de

Electronic Doping in Perovskite Solar Cells

*Zuzanna Molenda, Sylvain Chambon, Dario M. Bassani, and Lionel Hirsch**

The popularity of metal halide perovskites is in part the result of their versatility in numerous applications. To date, perovskites are used in their intrinsic, undoped form, as the doping of these materials is not yet adequately mastered. Herein, the recently reported electronic doping of $CH_3NH_3PbI_3$ is employed to fabricate perovskite solar cells in which the interfacial electron transport layer (ETL) is replaced by n-doping of one side of the perovskite film. The doping involves the incorporation of metastable Sm^{2+} ions that undergo an in situ oxidation to Sm^{3+}, releasing electrons to the conduction band to render the perovskite n-type. In spite of the lack of an ETL, these solar cells have the same efficiency as the samples with the ETL. The open circuit voltage of the doped solar cells increases proportionally to the doping concentration due to the narrowing of the depletion layer thickness at the interface of the perovskite and the top electrode, reaching the value of ≈1 V for the doped ETL-free device, the same as for the reference sample. These proof-of-concept results represent the first step toward perovskite-based devices incorporating a p-n homojunction.

1. Introduction

Metal halide perovskites are a recent class of semiconductors that has found applications in many devices, such as solar cells [1–5] light emitting diodes (LEDs),[6,7] photodetectors,[8,9] X-ray detectors[10] or transistors.[11–13] When made from inorganic semiconductors, such as Si or GaAs, these devices employ p and n doping to ensure the selectivity of charge injection or extraction. For perovskites, however, electrically efficient doping was achieved only recently, with only a few demonstrations on thin films.[14–16] A first example of the fabrication of a perovskite p-n diode has very recently been reported, using a co-evaporation method with organic dopants.[17] Herein, n-type perovskite doping is used in solar cell devices with the aim of demonstrating the first steps toward the use of a p-n homojunction thanks to the control of perovskite doping. A solar cell device was selected for this first demonstration of doping in a perovskite device due to the large body of knowledge in optimizing their architecture. With the latest record efficiency of the perovskite solar cells (PSC) being 26.1%,[18] they are approaching the Shockley-Queisser limit. The most important aspect toward the maximization of the cell performance has become the optimization of the fabrication parameters: from the choice of materials used to ensure the closest to ideal band alignment[19–21] to the seemingly negligible, such as the ambient temperature[22] or humidity.[23] Nowadays, PSC optimization is focused mainly on minimizing the non-radiative losses, the probable reason why the open circuit voltage (V_{OC}) of PSC is still below its theoretical limit. In order to minimize these losses, four main strategies have emerged: i) band alignment optimization,[20,21,24] ii) control of crystal growth,[25–27] iii) grain-boundary defect passivation,[28–30] and iv) interfacial defect passivation.[28,31] These strategies involve the incorporation of an interfacial layer selective for either hole (HTL) or electron (ETL) transport. While the selection of the charge transport materials with adapted electronic properties is crucial for the functioning of the solar cell, it can also be a limitation as the interfaces are naturally rich in defects that are often recombination sites. Hence, decreasing the number of layers could potentially minimize the losses and doping can be a way to simplify the PSC design. High resistance at the interfaces of perovskite solar cells can be decreased using ionic liquids or ammonium-based passivating layers. These strategies take advantage of the energy level alignment to improve the transport of electrons and holes to the electrical contacts. They can also result in the defect passivation and improved stability.[32–36]

The problem of high resistance at the interface with metals can be also solved by doping the perovskite material near the interface. However, efficient electrical doping of hybrid perovskite materials based on the incorporation mono- or tri-valent metal ions is not possible due to the ionic nature of the perovskite crystal. To circumvent this, we have recently reported the use of metastable samarium(II) ions that resulted in the n-type doping of $CH_3NH_3PbI_3$ (MAPI).[14] The incorporation of Sm^{2+} ions

Z. Molenda, S. Chambon, L. Hirsch
Univ. Bordeaux
CNRS
Bordeaux INP
IMS, UMR 5218, Talence F-33400, France
E-mail: lionel.hirsch@ims-bordeaux.fr
Z. Molenda, D. M. Bassani
Univ. Bordeaux
CNRS
Bordeaux INP
IMS, UMR 5255, Talence F-33400, France

The ORCID identification number(s) for the author(s) of this article can be found under https://doi.org/10.1002/aelm.202400090

DOI: 10.1002/aelm.202400090

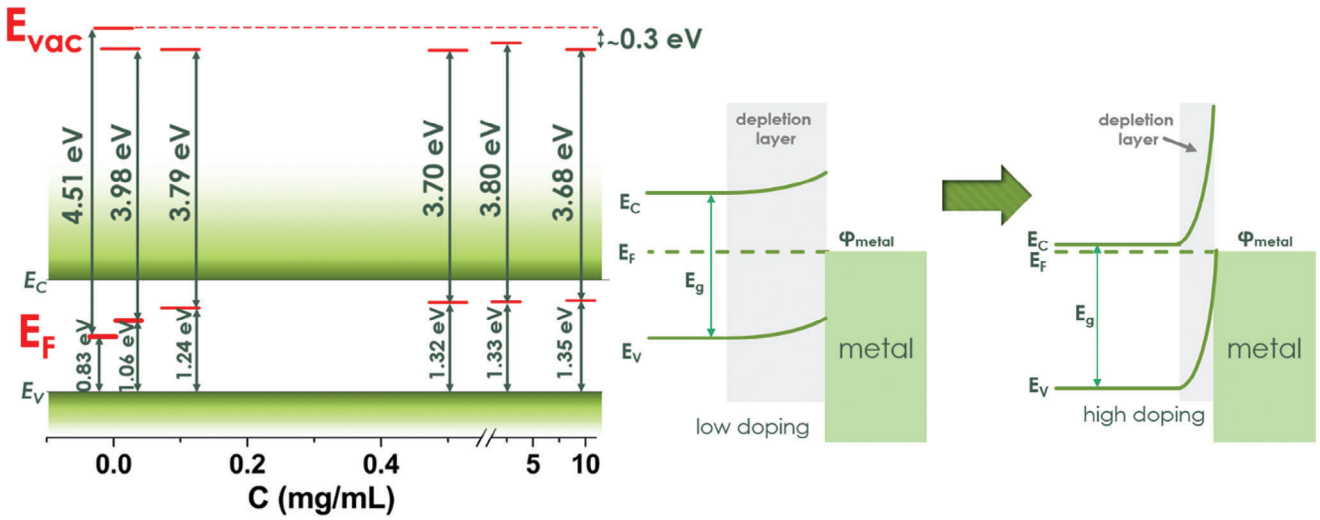

Figure 1. a) Variation of the E_F for doped MAPI as a function of the dopant concentration of the solution, result reprinted under a Creative Commons Attribution-NonCommercial 3.0 Unported Licence.[14] b) Schottky junction with a decrease of the depletion layer thickness as a function of doping concentration.

in the MAPI crystal structure is followed by their spontaneous oxidation to Sm^{3+} and the release of free electrons to the conduction band. In the present study, we apply this finding to the fabrication of solar cells that include n-type doping of the MAPI layer close to the electron-collecting electrode. We hypothesize that the high doping level (N_D) at the MAPI/metal interface leads to a decrease of the depletion layer thickness (w), which will be low enough for the electrons to tunnel (**Figure** 1b), according to the following equation:

$$w = \sqrt{\frac{2\epsilon}{qN_D}\left(V_{bi} - V\right)} \tag{1}$$

where ϵ is the dielectric permittivity, q is the elementary charge, V is the applied voltage and V_{bi} is the built-in potential. As shown before, the Fermi level (E_F) shifts from the middle of the bandgap for the undoped MAPI, to a level of ≈0.3 eV below the conduction band bottom (E_C), as reported in Figure 1a, independently to the anode work function. Therefore, whatever the metal electrode, we expect to have an ohmic contact at the anode. To confirm our statement and once again demonstrate that the properties of our material are consistent with classical electronic doping, we use a gold electrode with a high work function on the n-side of the device, even though it is typically used as a hole collector. Gold was chosen also due to the low chemical reactivity with MAPI. The concept of using doping in perovskite solar cells mimics the architecture used in silicon-based devices and has not been previously reported for these materials.

2. Results and Discussion

Samarium (II) iodide (SmI_2) is used as a source of Sm^{2+} ions. The concentration of the SmI_2 solution used in a two-step doping method (see the Supporting information for experimental details) was optimized for the thickness of the MAPI films used for the devices. As a quick estimation of charge carrier density, the conductivity of 190 nm-thick MAPI films was measured as a function of the concentration of the doping solution and is presented in **Figures** 2 and S1 (Supporting Information). One can clearly see the conductivity increase by two orders of magnitude upon doping of the pristine perovskite film with SmI_2. The conductivity reaches a maximum of 4×10^{-6} $\sigma.cm^{-1}$ for 3 mg mL^{-1} and decreases for higher concentrations. Based on this, concentrations of SmI_2 of 0.5, 1, 3, 5, and 7.5 mg mL^{-1} were selected for testing solar cells.

The architectures of the samples are presented in **Figure** 3. PCBM is used as an ETL for the reference samples. So far, to the best of our knowledge, there is no demonstration of efficient electrical p-type doping of MAPI. Very promising results on perovskite p-type doping have been reported by Euvrard et al.,[15] but their approach requires the use of perovskite with a high valence band maximum (VBM), such as the mixed-metal $MAPb_{0.5}Sn_{0.5}I_3$, which is much more challenging to use for preparing an efficient

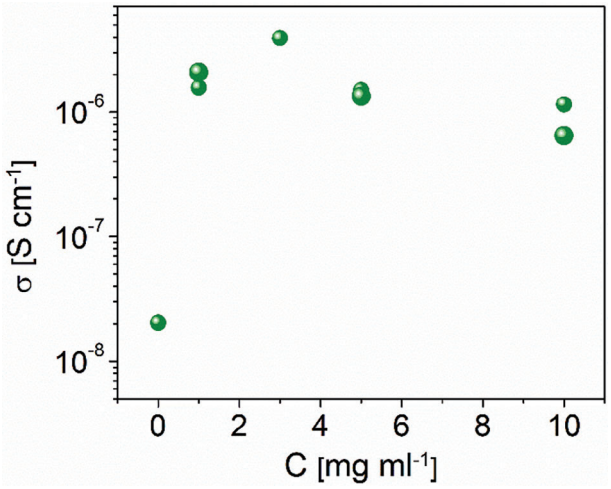

Figure 2. Conductivity as a function of the concentration of the doping solution.

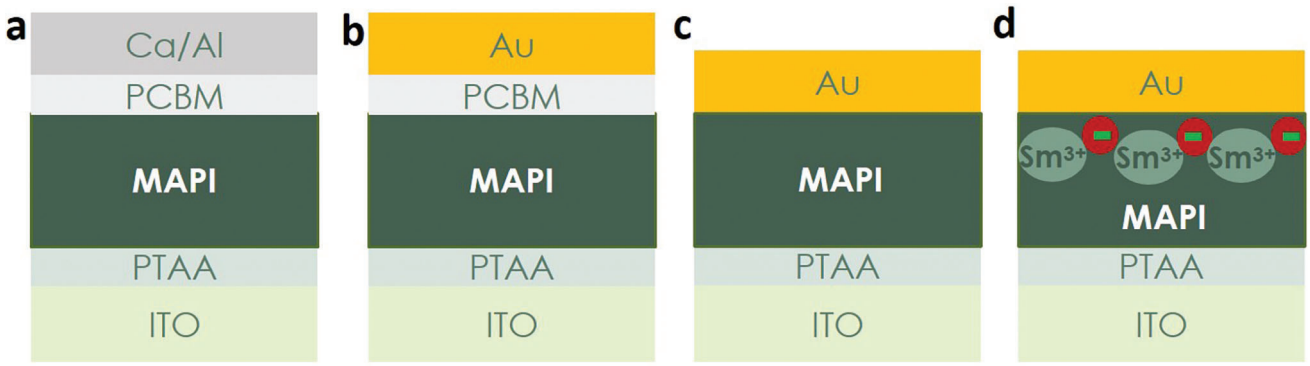

Figure 3. The architecture of the samples used in this study. a) Reference with PCBM as ETL and low WF electrode of Ca and Al, b) reference with PCBM as ETL and Au as electrode, c) undoped and ETL-free solar cell, d) solar cell with doped perovskite, using different concentrations of SmI_2.

and stable solar cell device. In this study, we therefore opted for the use of poly(triaryl amine) (PTAA) as the hole transporting layer (HTL). Importantly, the PTAA is not only an HTL but also an excellent electron-blocking layer, with an electron affinity close to −3 eV. This prevents the electrons to be collected by the cathode (here ITO), making the top metal electrode the only way out for electrons to the external circuit, resulting in the shunt resistance (R_{shunt}) of over 10 kOhm for all the solar cells (Figure S3, Supporting Information). Moreover, the work function (φ) of the ITO sets the position of the E_F of the much less conductive PTAA and perovskite closer to the E_V, with the hole density at the PTAA/perovskite interface higher than the electron density. This allows the transport of holes toward the ITO electrode. Therefore, as pointed out by Kirchartz et al.,[37] the electronic properties of the perovskite close to the interface with PTAA resemble those of p-doped semiconductor, even though the perovskite alone is intrinsic. N-type doping of such a stack could be then comparable to a p-n junction.

In order to minimize the risk of a metal and halide reaction at the junction, we use deposition of a gold electrode so the φ of the anode is higher than the one of the cathode. This unfavorable situation leads to almost canceling of the built-in potential, impeding the electron extraction. The high energy barrier for the electron injection in the forward bias obviously increases the R_{series}. This effect is even more pronounced when the ETL is removed and contributes to the increase of R_{series}, as demonstrated in Figure S3 (Supporting Information) and **Table 1**. Indeed, the average R_{series} of 750 Ω doubles when the ETL is removed (undoped sample) due to the high energy barrier between E_C of the perovskite and the φ of Au. The increase of the doping concentration leads to a decrease of the depletion layer, which results in the decrease of the R_{series}, as the probability of charge tunneling rises and the built-in potential increases. The minimum R_{series} is observed for 3 mg mL^{-1} and a slight increase can be attributed to the phase separation resulting from the over-doping, as suggested earlier [14] and consistent with the observed decrease in conductivity (Figure 2).

The impact of the doping on the V_{OC} is presented in **Figure 4a**. For the reference cells (with PCBM) with either Ca/Al and Au as an electrode, V_{OC} is close to 1 V, showing little impact of the top electrode on this parameter. It is interesting to note that when the ETL is removed and the devices should be hole-only with a high and similar work function of both electrodes and no built-in potential, their *I-V* characteristics are still diode-like with a non-negligible average V_{OC} of 0.54 ± 0.03 V, J_{SC} of 14.67 ± 0.32 mA cm^{-2}, and *FF* of 0.51 ± 0.03. This unexpected effect can be explained by the trapping of holes near the Au/MAPI interface at forward bias, as suggested by Chen et al.[38] Alternatively, it has been suggested by Kerner et al.[39] that the applied bias leads to the formation of Au^+ cations that can migrate through interstitial sites. The formation of ionized Au^{+1} species would necessarily result in the release of a negative charge that may induce partial n-doping of the perovskite at the Au/MAPI interface. Either of these phenomena can explain why the undoped solar cells possess some diode-like behavior.

Table 1. Main parameters of the solar cells with different top electrodes and different doping concentrations.

sample	R_{shunt} [kΩ]	R_{series} [Ω]	V_{OC} [V]	J_{SC} [mA cm^{-2}]	FF	PCE [%]
PCBM/Ca/Al	28.38 ± 13.67	113.01 ± 82.27	0.96 ± 0.05	19.71 ± 0.24	0.71 ± 0.04	13.42 ± 1.14
PCBM/Au	59.07 ± 76.07	785.44 ± 94.85	0.95 ± 0.03	17.73 ± 0.75	0.58 ± 0.02	9.87 ± 0.60
undoped	5997.69 ± 15467.00	1440.44 ± 176.40	0.54 ± 0.03	14.67 ± 0.32	0.51 ± 0.03	4.05 ± 0.39
0.5 mg mL^{-1}	1396.80 ± 1637.56	283.86 ± 129.98	0.66 ± 0.01	11.36 ± 0.79	0.57 ± 0.06	4.28 ± 0.56
1 mg mL^{-1}	343.57 ± 275.83	134.85 ± 81.07	0.73 ± 0.02	12.41 ± 0.83	0.59 ± 0.03	5.33 ± 0.57
3 mg mL^{-1}	154.77 ± 66.85	80.12 ± 31.49	0.93 ± 0.02	16.62 ± 0.97	0.63 ± 0.04	9.63 ± 0.75
5 mg mL^{-1}	81.10 ± 55.48	140.46 ± 22.47	0.94 ± 0.01	13.95 ± 1.49	0.57 ± 0.05	7.57 ± 1.19
7.5 mg mL^{-1}	14.96 ± 13.48	165.81 ± 24.20	0.88 ± 0.03	10.08 ± 1.48	0.47 ± 0.09	4.15 ± 0.99

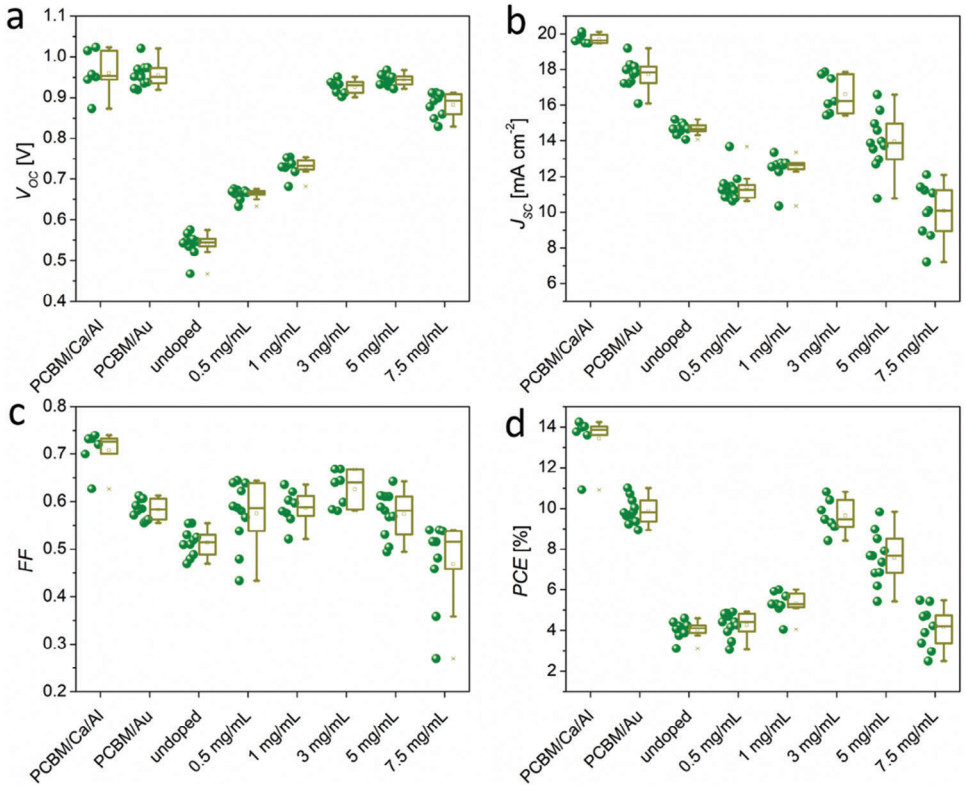

Figure 4. V_{OC} a), J_{SC} b), FF c), and PCE d) as a function of doping concentration.

As the doping concentration increases, the V_{OC} also gradually increases, finally reaching a maximum value that is similar to the one observed for the reference (PCBM/Ca/Al) device at the optimized doping concentration of 3 mg mL^{-1}. The increase of the V_{OC} with the doping concentration is a direct consequence of the shift of the MAPI Fermi level toward the conduction energy. It is worth noting that while the V_{OC} is not affected by the top electrode (the same V_{OC} for Ca/Al and Au), the short circuit current J_{SC} and the *FF* decrease on average by 1.98 mA cm^{-2} and 0.13, respectively. This is the result of the increased R_{series} due to the less favorable work function of the Au for electron extraction that creates a higher energy barrier for the electrons to overcome.

Taking into account that the doping is performed in a two-step process, that is, the dopant precursor (SmI_2) is deposited on the already formed perovskite, it is possible that a thin layer of residual SmI_2 may remain at the Au/MAPI interface. It would likely act as a barrier for the migration of Au^+ cations or reduce the formation of hole traps, thus minimizing the aforementioned doping effect on the undoped solar cells. For low concentrations of SmI_2, such as 0.5 and 1 mg mL^{-1}, this effect is manifested in the J_{SC} and *FF* being lower than for the undoped samples. For the doped solar cells, the highest J_{SC} and *FF* were achieved for the SmI_2 concentration of 3 mg mL^{-1}, with the values of 16.62 ± 0.97 mA cm^{-2} and 0.63 ± 0.04, respectively.

From the measured values of V_{OC}, J_{SC}, and *FF*, the power conversion efficiency (*PCE*) can be calculated and the values obtained are collected in Figure 4d. The *PCE* of the ETL-free solar cell with the doping concentration of 3 mg mL^{-1} (9.9 ± 0.7%) is comparable to the one with the PCBM as the ETL and the gold electrode (9.6 ± 0.8%). Low efficiencies of the undoped (4.0 ± 0.4%) and lightly doped (4.3 ± 0.6% and 5.3 ± 0.6% for 0.5 and 1 mg mL^{-1}, respectively) devices are a direct result of the drop of other parameters, described above. For doping concentrations higher than 3 mg mL^{-1}, notably 5 and 7.5 mg mL^{-1}, the solar cell parameters start to deteriorate (except for the V_{OC} for 5 mg mL^{-1}), which corresponds also to the decrease of the conductivity (Figure 2). As suggested in our previous work and supported from examination of XRD patterns, a high doping concentration results in a significant decrease in the crystallinity of the perovskite film which eventually impedes charge transport.

3. Conclusion

We present the first proof-of-concept example of using the n-doped methylammonium lead iodide perovskite for the fabrication of ETL-free solar cells. Solar cells with a PTAA layer on one side for hole-transport selectivity replaced the ETL layer on the anode side with the n-type perovskite region. For this proof-of-concept, we used a high work function gold electrode both to reduce the reactivity of the metal with the perovskite and to demonstrate once again the authenticity of the electronic n-type doping of the material, in its classical understanding and consistent with solid-state physics descriptors. For non-intentionally doped samples, we have shown that the Au/MAPI interface is not entirely electronically neutral, as some interaction resembling a slight n-type doping can occur. Nevertheless, as expected, we show a clear and obvious impact of intentional doping on solar cell behavior. For the optimized doping concentration, the ETL-free solar cells

display the same efficiency as those solar cells prepared with an optimized PCBM ETL layer and Au electrode. The observed increase of the V_{OC}, is proportional to the doping concentration and illustrates the gradual rising of the Fermi level and the narrowing of the depletion layer at the Au/perovskite interface until it is thin enough to allow the charge tunneling when the V_{OC} is the same as for the reference cells.

These results are the first step toward enabling the fabrication of the perovskite devices using efficient and well-controlled doping. We believe they can be an inspiration for what has so far seemed to be impossible in the domain of perovskite semiconductors–using doping to fabricate devices. While this is the first, proof-of-concept step, it is likely that other applications will start appearing soon, notably in the form of transistors, which still lack their perovskite homojunction-based representation.

4. Experimental Section

Materials: Lead(II) acetate trihydrate ($PbAc_2{\cdot}3H_2O$, 5N) was purchased from Sigma–Aldrich. Methylammonium iodide (CH_3CN_3I, > 4N) was purchased from GreatCell Solar Materials. Samarium(II) iodide (SmI_2, 4N) was purchased from Alfa Aesar. Poly(triaryl amine) (PTAA) with a molecular weight of 17 kDa was purchased from Solaris Chem. Phenyl-C_{61}-butyric acid methyl ester (PCBM, 4N) was purchased from Solaris. Anhydrous toluene, anhydrous *N,N*-Dimethylformamide (DMF), and anhydrous chlorobenzene (CB) were purchased from Sigma–Aldrich.

Substrates: For the conductivity measurements, glass substrates with patterned gold electrodes were used. For fabricating the solar cells, glass substrates covered with a thin layer of ITO (10 Ω sq^{-1}) were selected.

Sample Fabrication: The substrates were cleaned in a sonication bath first with Hellmanex™ III solution (Sigma–Aldrich) and in DI water for 15 min each and then in isopropanol (4N) for 10 min. Subsequently, they were treated with a UV-ozone for 15 min. Sample fabrication was performed under a controlled atmosphere in a glove box. 4.5 mg PTAA was dissolved in toluene, stirred at RT overnight, and filtered with a 0.45 µm PTFE filter. The 15 nm thick PTAA layer was spin coated onto clean substrates at a spin rate of 6000 rpm for 30 s and dried for 10 min at 100 °C. The perovskite precursor solution was prepared by dissolving 0.72 M $PbAc_2{\cdot}3H_2O$ and 2.2 M MAI in DMF and stirring at room temperature for 30 min. The solution was filtered through a 0.45 µm PTFE filter and spin coated at a spin rate of 6000 rpm for 2 min. The sample was then dried at RT for 3 min and annealed for 25 min at 100 °C. The perovskite film thickness was ≈190 nm. SmI_2 was dissolved in isopropanol and DMF (0.1% v v^{-1}) and stirred overnight at RT. The solution was filtered with a 0.45 µm PTFE filter and spin coated at a spin rate of 2500 rpm for 1 min. The sample was placed on the hot plate at 100 °C for 10 min. 20 mg PCBM was dissolved in CB and stirred overnight at 50 °C. After being filtered with a 0.45 µm PTFE filter, the solution was spin coated at spin rate of 2500 nm for 1 min, resulting in a layer thickness of ≈90 nm. The electrodes 30 nm Ca and 70 nm Al or 100 nm Au were thermally evaporated, using a mask that defined the area of the cells.

Characterization: Conductivity was calculated from the *I–V* curves that were collected using a Keithley 4200 source meter unit (SMU). The samples were scanned from −1 to 1 V at a rate of 5 mV s^{-1}. The IV curves were registered using a Keithley 2400 source meter unit (SMU) controlled by a homemade LabView program. The solar cell devices were scanned from -1 to 1.2 V with the rate of 10 mV s^{-1}. The solar simulator Oriel LCS-100™ Small Area Sol1A with class ABB, as defined by the ASTM and IEC standards, was used with the AM 1.5G spectrum and irradiance set at 100 mW cm^{-2} with the Oriel 91150 V Reference Cell. The active solar cell area is 10.5 mm^2. No mask was used for the measurement; however, the cells were separated from one another by mechanical etching between the electrodes to block the current flow from the neighboring cells.

Supporting Information

Supporting Information is available from the Wiley Online Library or from the author.

Acknowledgements

This research was funded by the Agence Nationale de la Recherche (HYPERSOL project no. ANR-18-CE05-0021-01) and the Region Nouvelle Aquitaine (STRIPE project no. 2019-1R1M08).

Conflict of Interest

The authors declare no conflict of interest.

Data Availability Statement

The data that support the findings of this study are available from the corresponding author upon reasonable request.

Keywords

doping, n-type, perovskite, solar cells

Received: February 8, 2024
Revised: April 17, 2024
Published online:

[1] Z. K. Tang, Z. F. Xu, D. Y. Zhang, S. X. Hu, W. M. Lau, L. M. Liu, *Sci. Rep.* **2017**, *7*, 7843.
[2] D. J. Kubicki, D. Prochowicz, A. Hofstetter, S. M. Zakeeruddin, M. Grätzel, L. Emsley, *J. Am. Chem. Soc.* **2017**, *139*, 14173.
[3] S. De Wolf, J. Holovsky, S. J. Moon, P. Löper, B. Niesen, M. Ledinsky, F. J. Haug, J. H. Yum, C. Ballif, *J. Phys. Chem. Lett.* **2014**, *5*, 1035.
[4] D. Barrit, P. Cheng, M. C. Tang, K. Wang, H. Dang, D. M. Smilgies, S. Liu, T. D. Anthopoulos, K. Zhao, A. Amassian, *Adv. Funct. Mater.* **2019**, *29*, 1807544.
[5] X. Wen, Y. Feng, S. Huang, F. Huang, Y. B. Cheng, M. Green, A. Ho-Baillie, *J. Mater. Chem. C* **2015**, *4*, 793.
[6] S. Sandrez, Z. Molenda, C. Guyot, O. Renault, J. P. Barnes, L. Hirsch, T. Maindron, G. Wantz, *Adv. Electron. Mater.* **2021**, *7*, 2100394.
[7] X. Zhang, W. Wang, B. Xu, S. Liu, H. Dai, D. Bian, S. Chen, K. Wang, X. W. Sun, *Nano Energy* **2017**, *37*, 40.
[8] D. M. Jang, K. Park, D. H. Kim, J. Park, F. Shojaei, H. S. Kang, J. P. Ahn, J. W. Lee, J. K. Song, *Nano Lett.* **2015**, *15*, 5191.
[9] B. Yang, F. Zhang, J. Chen, S. Yang, X. Xia, T. Pullerits, W. Deng, K. Han, *Adv. Mater.* **2017**, *29*, 1.
[10] K. Sakhatskyi, B. Turedi, G. J. Matt, E. Wu, A. Sakhatska, V. Bartosh, M. N. Lintangpradipto, R. Naphade, I. Shorubalko, O. F. Mohammed, S. Yakunin, O. M. Bakr, M. V. Kovalenko, *Nat. Photonics* **2023**, *17*, 510.
[11] W. Yu, F. Li, L. Yu, M. R. Niazi, Y. Zou, D. Corzo, A. Basu, C. Ma, S. Dey, M. L. Tietze, U. Buttner, X. Wang, Z. Wang, M. N. Hedhili, C. Guo, T. Wu, A. Amassian, *Nat. Commun.* **2018**, *9*, 1.
[12] A. Liu, H. Zhu, S. Bai, Y. Reo, T. Zou, M. G. Kim, Y. Y. Noh, *Nat. Electron.* **2022**, *5*, 78.
[13] X. Y. Chin, D. Cortecchia, J. Yin, A. Bruno, C. Soci, *Nat. Commun.* **2015**, *6*, 7383.
[14] Z. Molenda, B. Politi, R. Clerc, M. Abbas, S. Chambon, D. M. Bassani, L. Hirsch, *Mater. Horiz.* **2023**, *10*, 2845.

[15] J. Euvrard, O. Gunawan, X. Zhong, S. P. Harvey, A. Kahn, D. B. Mitzi, *Mater. Adv.* **2021**, *2*, 2956.
[16] Z. Fang, H. He, L. Gan, J. Li, Z. Ye, *Adv. Sci.* **2018**, *5*, 1800139.
[17] T. Schramm, M. Deconinck, R. Ji, E. Siliavka, Y. J. Hofstetter, M. Löffler, V. V. Shilovskikh, J. Brunner, Y. Li, S. Bitton, N. Tessler, Y. Vaynzof, *Adv. Mater.* **2024**, 2314289.
[18] J. Park, J. Kim, H. S. Yun, M. J. Paik, E. Noh, H. J. Mun, M. G. Kim, T. J. Shin, S. Il Seok, *Nature* **2023**, *616*, 724.
[19] M. Caputo, N. Cefarin, A. Radivo, N. Demitri, L. Gigli, J. R. Plaisier, M. Panighel, G. Di Santo, S. Moretti, A. Giglia, M. Polentarutti, F. De Angelis, E. Mosconi, P. Umari, M. Tormen, A. Goldoni, *Sci. Rep.* **2019**, *9*, 15159.
[20] Q. Jiang, X. Zhang, J. You, *Small* **2018**, *14*, 1801154.
[21] D. Saranin, P. Gostischev, D. Tatarinov, I. Ermanova, V. Mazov, D. Muratov, A. Tameev, D. Kuznetsov, S. Didenko, A. Di Carlo, *Materials* **2019**, *12*, 1406.
[22] Z. Molenda, S. Chambon, D. M. Bassani, L. Hirsch, *Eur. J. Inorg. Chem.* **2021**, *2021*, 2533.
[23] I. Mesquita, L. Andrade, A. Mendes, *Sol. Energy* **2020**, *199*, 474.
[24] N. D. Pham, C. Zhang, V. T. Tiong, S. Zhang, G. Will, A. Bou, J. Bisquert, P. E. Shaw, A. Du, G. J. Wilson, H. Wang, *Adv. Funct. Mater.* **2019**, *29*, 1.
[25] T. Zhang, N. Guo, G. Li, X. Qian, Y. Zhao, *Nano Energy* **2016**, *26*, 50.
[26] S. Singh, D. Kabra, *J. Mater. Chem. C* **2018**, *6*, 12052.
[27] C. Pereyra, H. Xie, M. Lira-Cantu, *J. Energy Chem.* **2021**, *60*, 599.
[28] F. Wang, Y. Chen, G. Han, Q. Zhang, Q. Ma, *Curr. Appl. Phys.* **2016**, *16*, 1353.
[29] J. an Yang, A. Xiao, L. Xie, K. Liao, X. Deng, C. Li, A. Wang, Y. Xiang, T. Li, F. Hao, *Electrochim. Acta* **2020**, *338*, 135697.
[30] N. K. Noel, A. Abate, S. D. Stranks, E. S. Parrott, V. M. Burlakov, A. Goriely, H. J. Snaith, *ACS Nano* **2014**, *8*, 9815.
[31] J. Wang, K. Datta, C. H. L. Weijtens, M. M. Wienk, R. A. J. Janssen, *Adv. Funct. Mater.* **2019**, *29*, 1905883.
[32] X. Zhu, M. Du, J. Feng, H. Wang, Z. Xu, L. Wang, S. Zuo, C. Wang, Z. Wang, C. Zhang, *Angew. Chem., Int. Ed.* **2021**, *60*, 4238.
[33] C. Luo, G. Li, L. Chen, J. Dong, M. Yu, C. Xu, Y. Yao, M. Wang, Q. Song, S. Zhang, *Sustain. Energy Fuels* **2020**, *4*, 3971.
[34] W. Zhang, X. Liu, B. He, Z. Gong, J. Zhu, Y. Ding, H. Chen, Q. Tang, *ACS Appl. Mater. interfaces* **2020**, *12*, 4540.
[35] L. Shi, H. Yuan, X. Sun, X. Li, W. Zhu, J. Wang, L. Duan, Q. Li, Z. Zhou, Z. Huang, *ACS Appl. Energy Mater.* **2021**, *4*, 10584.
[36] P. Hu, S. Huang, M. Guo, Y. Li, M. Wei, *ChemSusChem* **2022**, *15*, 202200819.
[37] L. Krückemeier, B. Krogmeier, Z. Liu, U. Rau, T. Kirchartz, *Adv. Energy Mater.* **2021**, *11*, 2003489.
[38] Y. F. Chen, Y. T. Tsai, D. M. Bassani, R. Clerc, D. Forgács, H. J. Bolink, M. Wussler, W. Jaegermann, G. Wantz, L. Hirsch, *J. Mater. Chem. A* **2016**, *4*, 17529.
[39] R. A. Kerner, A. V. Cohen, Z. Xu, A. R. Kirmani, S. Y. Park, S. P. Harvey, J. P. Murphy, R. C. Cawthorn, N. C. Giebink, J. M. Luther, K. Zhu, J. J. Berry, L. Kronik, B. P. Rand, *Adv. Mater.* **2023**, *35*, 2302206.